



Numerical and Analytical Study on Bending Stiffness of Sandwich Panels at Ambient and Elevated Temperatures

Shoushtarian Mofrad, Ashkan^{1*} 

Pasternak, Hartmut¹ 

¹ Brandenburg University of Technology, Cottbus, Germany

Correspondence:* email ashkan.shoushtarianmofrad@b-tu.de; contact phone [+4917640454099](tel:+4917640454099)

Keywords:

Sandwich panels; Bending stiffness; Analytical study; Finite element analysis; Parametric study; Elevated temperatures

Abstract:

This paper presents an investigation on the bending stiffness of sandwich panels at ambient and elevated temperatures. A finite element (FE) model is developed to verify simulations with experimental results, and then a parametric study at different temperatures is carried out. After that, an analytical study to determine the bending stiffness at room temperatures according to the current specification is conducted. Furthermore, the analytical solutions are developed to use at elevated temperatures. The objective of the current research is to compare the numerical and analytical results. It is observed that analytical solutions developed to evaluate the bending stiffness at elevated temperatures are conservative and reliable.

1 Introduction

Sandwich panels can be employed efficiently to provide further stability to individual structural members (beams and columns) and entire building frames. In the STABFI (Steel cladding systems for stabilization of steel buildings in fire) project, it has been shown that in the case of fixed column bases and unprotected columns, the fire resistance of steel frames with steel claddings (no bracings) is 22% higher than with only traditional bracings (Fig. 1). It shows that the steel claddings systems provide better stabilization in a fire case [1]. Although there is a broad range of design codes to predict the bending stiffness of sandwich panels at ambient temperature, the knowledge of their performance at elevated temperatures is not still explicit.

Sandwich panels, typically composed of two thin reinforced steel sheets bonded on each side of a thick and light-weight foam core, are used in industrial and commercial buildings. The core of a sandwich structure can vary in material. Generally, the cores divide into four types, foam or solid core, honeycomb core, web core and corrugated or truss core [2,3]. In this research, the sheets are fabricated of steel along with mineral wool (MW) core. The cores are thick and light-weight materials whose primary role is to keep the sheets separated and make the whole structure resistant to vertical deformations [4]. Conversely, the sheets are thin and stiff materials whose function is to carry bending and in-plane forces [5]. Like many other research papers, in this study, the sandwich panels are subjected to bending loads [6,7,8,9,10,11].

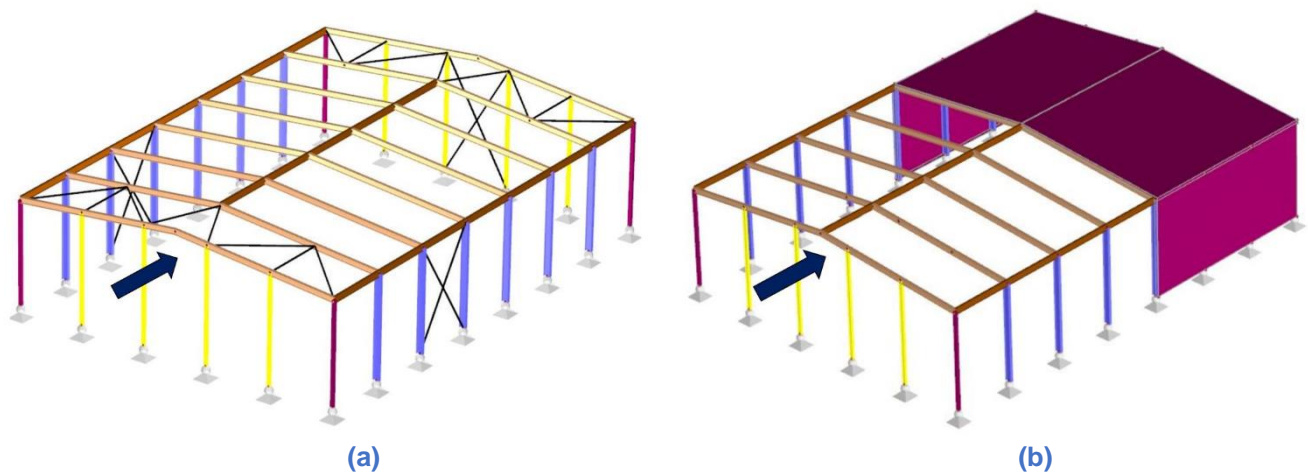


Fig. 1 - Portal frame structure: a) without steel claddings with the bracing system, b) without bracing system with steel claddings [1]

The bending stiffness and resistance of PIR and MW sandwich panels at room and elevated temperatures were discussed in [12,13]. Srivaro et al. [14] presented a study of the bending stiffness and strength of oil palmwood (OPW) core sandwich panel overlaid with rubberwood veneer under centre point bending loads. They used linear elastic beam theory to predict the bending performance of the panels. Results showed that the linear elastic beam theory using the power-law expressions of Young's modulus and shear strength of the OPW as a function of density adequately predicted the stiffness and bending strength of the sandwich beams. Joseph et al. [15] carried out experimental and analytical studies to understand and compare the flexural behaviour of concrete sandwich panels under two different loading conditions, such as punching and four-point bending. The experimental study indicated that the type of loading conditions affects the flexural behaviour of the concrete sandwich panels significantly. The results of an experimental and statistical comparative analysis of "Fire Reaction" development in sandwich panels consisting of steel sheeting and Polyisocyanurate (PIR) foam core were presented by Murillo et al. [16]. They proved that there is an effect of the sample thickness in the results of the "Single Burning Item" (SBI) test parameters; however, this variability has no significant influence on the "Fire Reaction" performance of the samples. Vignesh Iyer et al. [17] carried out a comparative study between the three-point and four-point bending of rigid glass epoxy sandwich composites.

The purpose of this research is to evaluate the accuracy and reliability of the analytical formulation provided by Eurocodes (EN 14509, 2013) [18] to determine the bending stiffness of sandwich panels at room temperature. Besides, the analytical formulation is developed to apply at elevated temperatures. Therefore, after verifying simulations with the experimental results, a parametric study for normal and elevated temperatures is conducted. During the parametric study, the decisive components such as height, length and width of the panel, also the thickness of sheets, are changed and investigated.

2 Materials and Methods

2.1 Experimental program

The objective of the experimental program was to determine the bending stiffness of MW sandwich panels under bending loading at normal and elevated temperatures. The tests were carried out at the laboratory of the Faculty of Civil Engineering, Czech Technical University in Prague. The inner and outer sheet thickness for MW panels is 0.5 mm and 0.6 mm, respectively, and its width was 1200 mm. The height of the panel varied between 100 mm and 230 mm. Fig. 2 shows the test arrangement and applied dimensions of specimens [19].

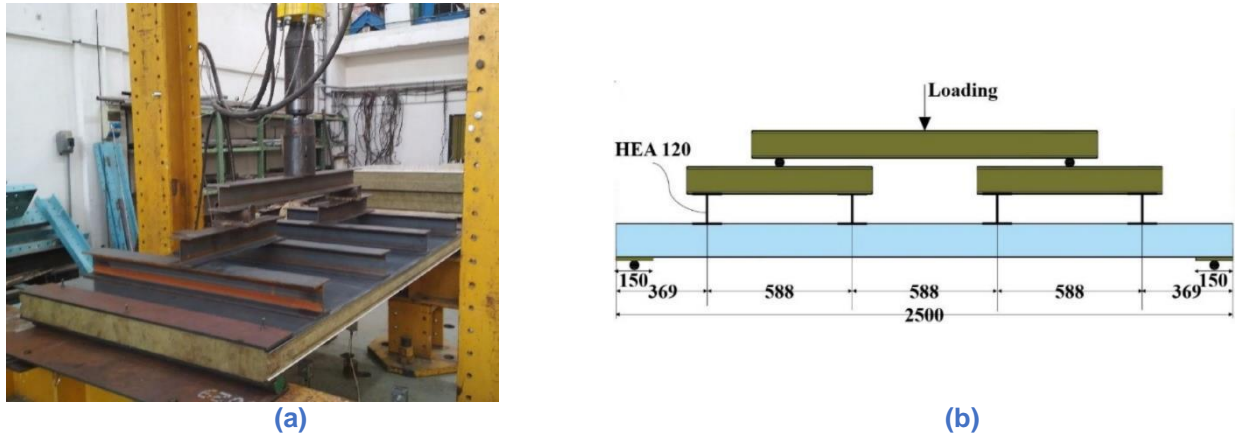


Fig. 2 - Test arrangement of MW panel, a) test, b) dimensions in mm

As shown in Fig. 2, the bottom of the panel was fixed at both sides, and the load was applied by a hydraulic jack from the upper side through four HEA120 beams. The loading rate was set to a constant value of 0.050 mm per second (mm/s) or 0.075 mm/s. A system of ceramic heating pads was employed to heat the bottom surface of the inner steel sheet. The heating pads were uniformly distributed on the inner sheet of the panel (Fig. 3). The temperature of the inner panel face was controlled by coated thermocouples. Besides, the heating pads were covered by insulation materials to prevent wasting the heat. The specimens were tested at different temperatures of 20, 300, 450, 600 °C [19].

Nine coated thermocouples recorded the inner sheet's temperature (lower side during the test). The outer sheet's temperature was measured by three thermocouples. The temperature of the panel core was recorded with six thermocouples (Fig. 3). Thermocouples were located in half of the panel thickness and 1/5 of the panel core thickness. The loading order is as follows: first, a preload was applied to keep different parts in contact, and then, the panel was heated from the bottom. After reaching the desired temperature, mechanical loading was applied from the top of the panel while the temperature was maintained [19].

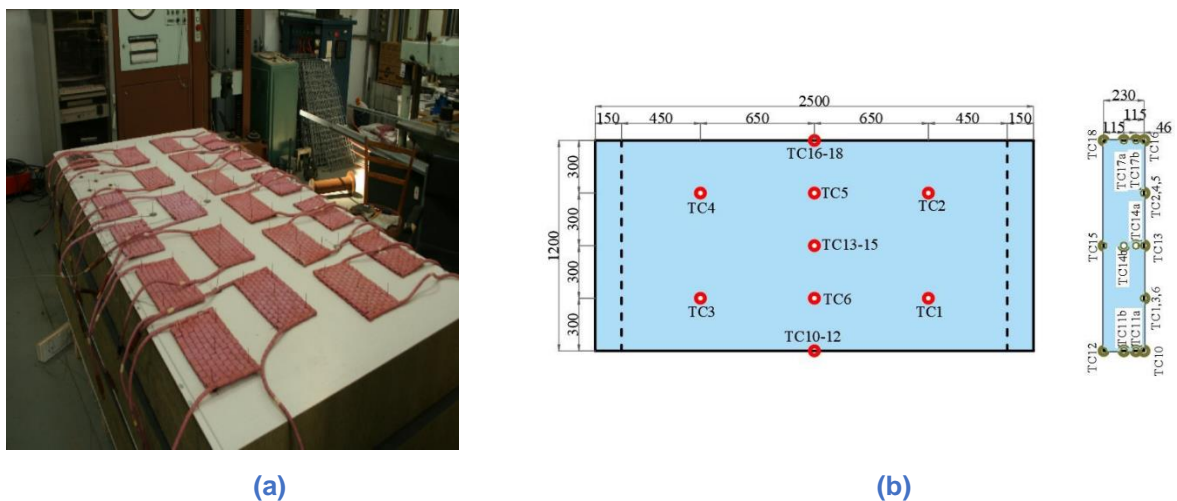


Fig. 3 - a) Distribution of ceramic heating pad on the panel face, b) Location of thermocouples dimensions in mm

During the tests, the displacements, the loading forces and the temperatures were measured. Temperatures were recorded by coated thermocouples, and deflections were measured by transducers. The applied force was taken by the testing machine. The experimental results are discussed and compared with the simulations in 2.3.5.

2.2 Analytical study

The static behaviour of single-span sandwich panels is illustrated by the expressions for the stress resultants and deflections caused by a uniformly distributed load given in EN 14509, Table E.10.1 [18]. To determine the bending stiffness of single-span sandwich panels, the applied load is divided by the maximum deflection (Eq. (2)). According to EN 14509, the maximum deflection and bending stiffness of the single-span sandwich panel at room temperature are calculated with Eq. (1) and Eq. (2), respectively.

$$v_{max} = \frac{5qL^4}{384B_s}(1 + 3.2k), \quad F = q \cdot L \Rightarrow v_{max} = \frac{5FL^3}{384B_s}(1 + 3.2k) \quad (1)$$

$$k_b = \frac{F}{v_{max}} = \frac{384B_s}{5L^3(1 + 3.2k)} \quad (2)$$

Where v_{max} , L , k_b , q , and F are the maximum deflection and the span of the panel, the bending stiffness, the uniform load and the concentrated load. B_s and k are defined based on Eq. (3) and Eq. (4).

$$B_s = \frac{E_{F1}A_{F1}E_{F2}A_{F2}e^2}{(E_{F1}A_{F1} + E_{F2}A_{F2})} \quad (3)$$

$$k = \frac{3B_s}{L^2G_cA_c} = \frac{3B_s}{L^2G_cbD} \quad (4)$$

Eq. (3) and Eq. (4) employ the following notations:

G_c	Shear modulus of core material,
A_c	The cross-sectional area of the core,
E_{F1}, E_{F2}	Young's modulus of the external and internal faces, respectively,
A_{F1}, A_{F2}	Cross-sectional areas of the external and internal faces, respectively,
E	The distance between the centroids of faces,
b, D	The width and height of the core.

Therefore, the bending stiffness of sandwich panels at ambient temperature is calculated by Eq. (2). In the fire case, the analytical formulation is modified by replacing Young's modulus of the exposed face and the shear modulus of the core material with the corresponding values at elevated temperatures. Due to the thin thickness of the inner steel sheet, the whole sheet thickness's temperature is constant (exposed temperature). As a result, Young's modulus of the inner sheet is a specific value calculated by the degradation of steel materials. However, the temperature distribution along the core thickness is different. As a matter of fact, the heat varies between the maximum temperature (exposed side) and room temperature (unexposed side). In such a case, it is proposed to use an average shear modulus of the core. This average value is computed according to the thickness ratio of each temperature layer. As a conservative approach, the shear modulus value can be calculated based on the shear modulus at the maximum core temperature. In 2.4, the analytical and numerical results are compared.

2.3 Numerical modelling

2.3.1 Model description

The finite element software ABAQUS [20] is utilized to develop a numerical model in order to simulate the bending tests. The main objective of the numerical study herein is first to verify the simulations with experiments and then to conduct a parametric study and compare the results with analytical ones. To simulate the behaviour of experimental specimens, a combination of heat transfer and mechanical analysis is performed. Indeed, the outputs of heat transfer analysis are the temperature distributions of specimens, which are applied as inputs of mechanical analysis. Load-displacement curvatures at different temperatures are the final outputs of the analysis. The main components of the developed finite element models are core and internal and external facings. The geometrical and material

nonlinearity for the model is considered. The dimensions of all models are created accurately in accordance with the geometry of experiments (2.1). At room temperature, the core and the facings are tied together in all directions. To reduce the shear resistance between the lower facing and core at elevated temperatures, in a core layer close to the interaction, the stiffness and material properties of the core are significantly decreased. This mechanism is applied as an alternative to consider delamination effects and reduce the computing time.

2.3.2 Material properties

A tensile coupon test was performed in the laboratory of the Department of Structural Engineering, Budapest University of Technology and Economics at ambient temperature to obtain steel material characteristics of the facings (Fig. 4). For simulation, a nonlinear isotropic/ kinematic hardening model is employed for both steel facings. This model adopts a typical elastic-plastic isotropic model, which follows the von Mises yielding criteria to define its isotropic yielding [21]. The tensile stress-strain behaviours of steel materials consider the strain hardening effect. At elevated temperatures, the mechanical properties of steel are reduced, according to the reduction factors presented by Craveiro et al. [22]. Thermal properties of the steel facings, such as thermal conductivity and specific heat, are taken from EN 1993-1-2 [23].

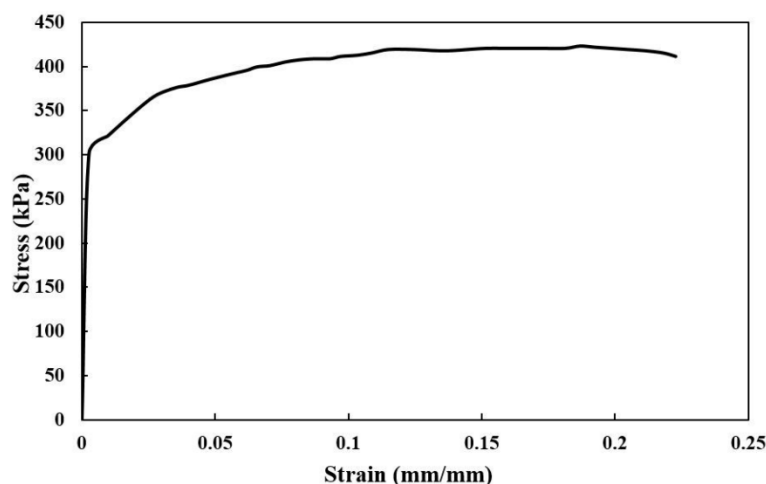


Fig. 4 - Stress-strain curve for the steel sheet at normal condition

The mechanical characteristics of polymer products may be described in terms of their density [24,25]. For this reason, the mechanical properties of MW cores were achieved from the tests. MW cores are usually orthotropic. Nonetheless, for simplicity, after comparing outputs of orthotropic and isotropic materials and observing negligible differences between numerical results, the cores are considered as isotropic materials in this research (Fig. 5). Degradation of core materials at elevated temperatures is based on the suggested reduction factor for Young's modulus of the MW core at elevated temperatures (Table 1). Thermal properties of MW cores are obtained from [26]. In the FE models, the engineering stresses and engineering strains are converted into the corresponding true stresses and true plastic strains for different temperatures [20].

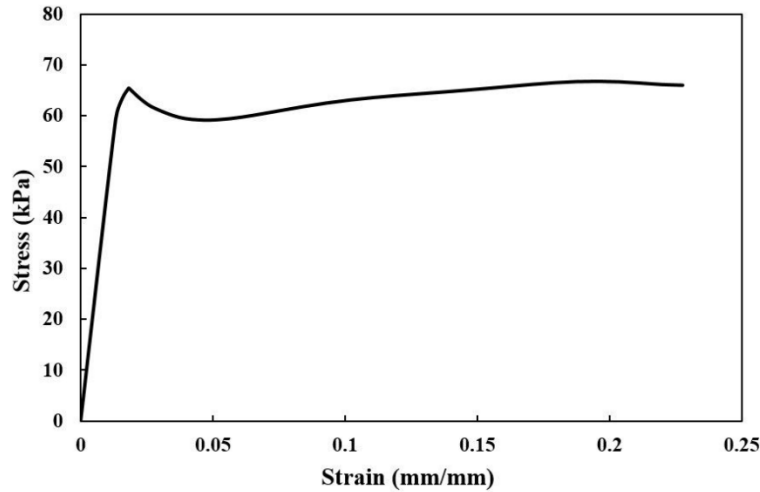


Fig. 5 - Stress-strain curve for the MW core

Table 1. The proposed reduction factor for Young's modulus of the MW core at elevated temperatures

Temperature (°C)	20	150	300	450	600
Reduction factor	1	0.75	0.5	0.25	0.25

2.3.3 Loading and boundary conditions

In order to simplify the numerical model, the load-transferring mechanism, including HEA120 beams and steel sections fixed to the sandwich panels, is removed. As an alternative, the loadings are directly applied to the upper side of the panel in four bands in the vertical direction. The areas and distances of the bands are similar to the experiments. Moreover, the lower face of the panel on a surface of 150 mm × 1200 mm at both ends are fully constrained ($U_x = U_y = U_z = 0$), where U is displacement (see Fig. 6). In the heat transfer analysis, as shown in Fig. 6, the temperature is assigned to the lower side of the bottom facing (the exposed side). The other parts of the specimens are in contact with ambient temperature.

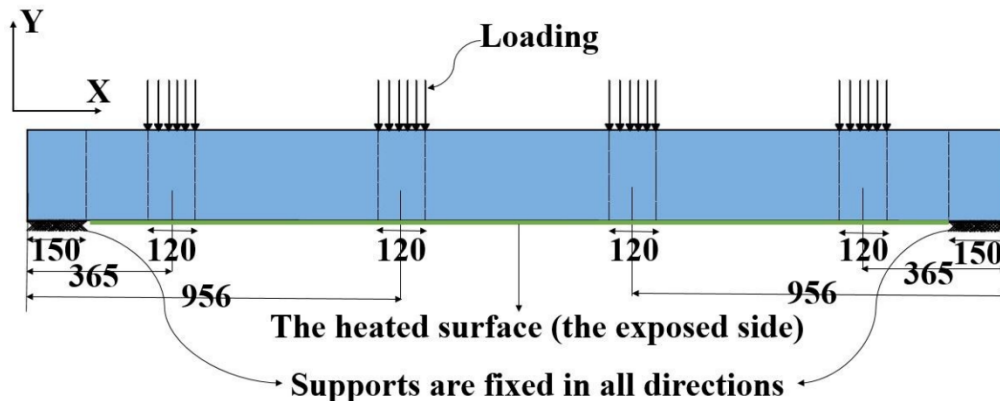


Fig. 6 - Boundary conditions and loadings of FE models

2.3.4 Element and mesh size

The continuum element C3D8R with hourglass control and reduced integration point is adopted to simulate the core material in the mechanical analysis. The C3D8R element is an 8-node linear brick element [20,21,27]. The element type for the facings is the S4R shell element, a 4-node doubly curved thin or thick shell with reduced integration, hourglass control and finite membrane strains [20,28,29,30,31].

In the heat transfer analysis, the DCC3D8 element is adopted for the core. The upper and lower facings are simulated by the DS4 element. The DCC3D8 is an 8-node convection/diffusion brick solid element, while the DS4 element is a 4-node heat transfer quadrilateral shell [20,31,32].

Mesh verification and sensitivity analyses are conducted to optimize the number of elements and meet favourable quality. In both heat transfer and mechanical analyses of each specimen, the size and number of the elements are accurately similar. In general, the mesh size is 30 mm × 20 mm × 10 mm in X, Y and Z directions, respectively. However, in an area with 428 mm length in the X direction from both ends of the panel, the element size is reduced to 10 mm × 20 mm × 10 mm. The area mentioned above is selected because of the observation from the experiments. Almost all failures and cracks initiation of panels have occurred within this area. Fig. 7 demonstrates the mesh quality of the whole sandwich panel model.



Fig. 7 - Element size in the numerical model

2.3.5 Validation of FE models

The experimental results are employed to validate the FE models. The validated models can be used in further parametric studies. The mode of failure and the load-displacement curvatures obtained from the experimental results and simulations are applied for comparison. The collapse of MW sandwich panels is usually caused by shear failure. Fig. 8 compares the failure mode of the test and a corresponding finite element model at ambient temperature. As can be seen, the area in the vicinity of the supports has the maximum yield stress.

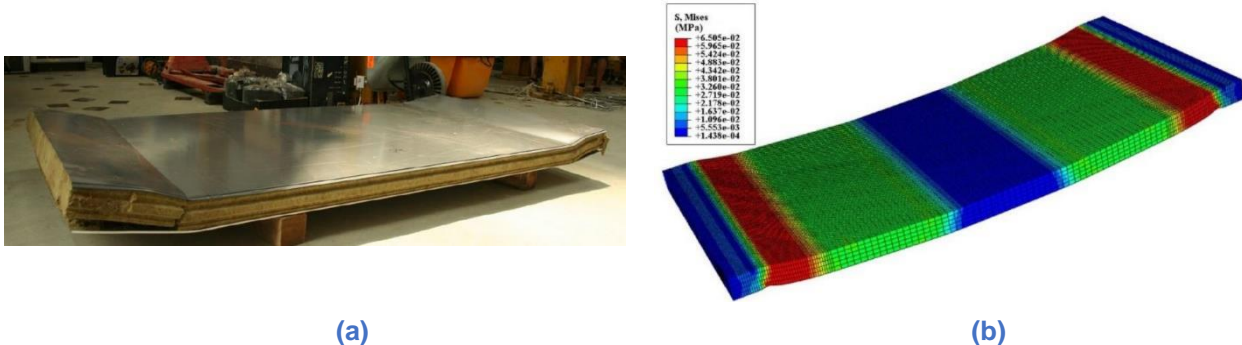


Fig. 8 - The failure mode for a) the test, b) the simulation

Fig. 9 shows the temperature distribution of experimental and numerical results for the sandwich panel with 230 mm thickness and the temperature of 600 °C at the exposed side [19]. For the steel sheets in the experiment and the simulation, the temperatures are evaluated in the middle of the plate. For the core material, the evaluation takes place in the middle of the core thickness. During the simulation, the plate's lower surface (exposed surface) is exposed to the measured temperature from the experiment (blue curve in Fig. 9). The room temperature was assigned to all other component surfaces at the beginning of the simulation. As shown in Fig. 9, there is an excellent agreement between the measured and simulated temperature profiles.

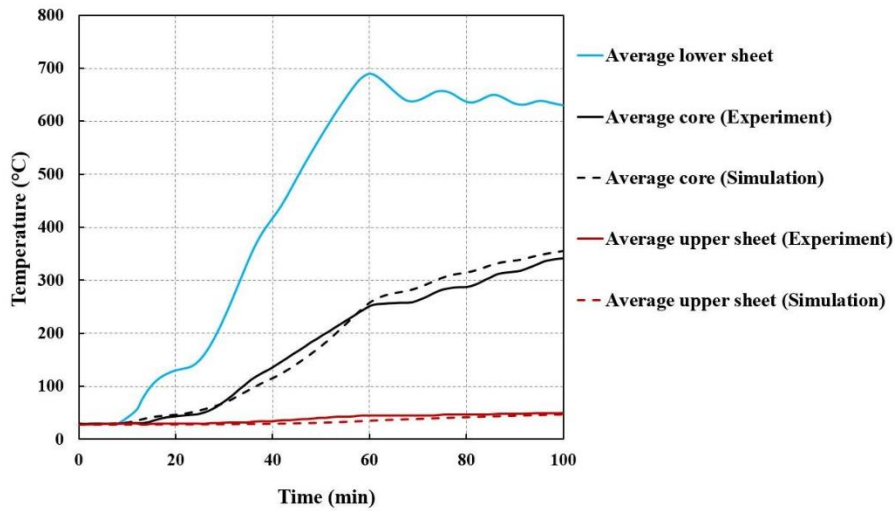


Fig. 9 - Temperature distribution from experiment and simulation for MW sandwich panels of 230 mm at 600°C

In Fig. 10 and Fig. 11, the load-displacement curvatures from experimental and numerical results for the 100 mm and 230 mm panels thickness are compared, respectively [19]. The displacement is taken from the centre of the lower sheet in the load direction, and the load presents the reaction force of supports. The geometry of sandwich panels is according to 2.1.

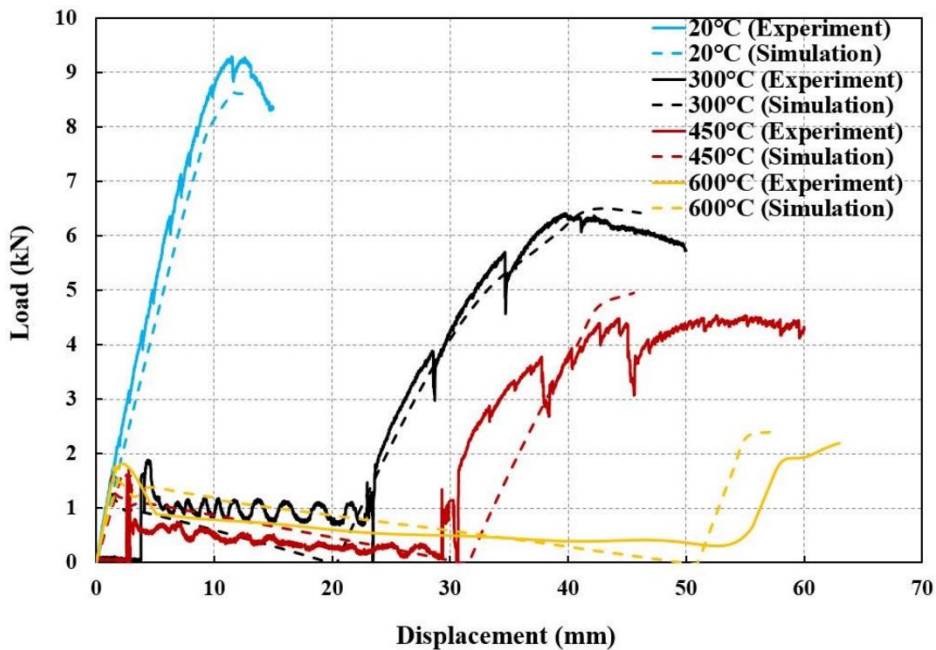


Fig. 10 - Comparison of load-displacement curves with MW panels 100 mm at different temperatures for experimental and numerical results

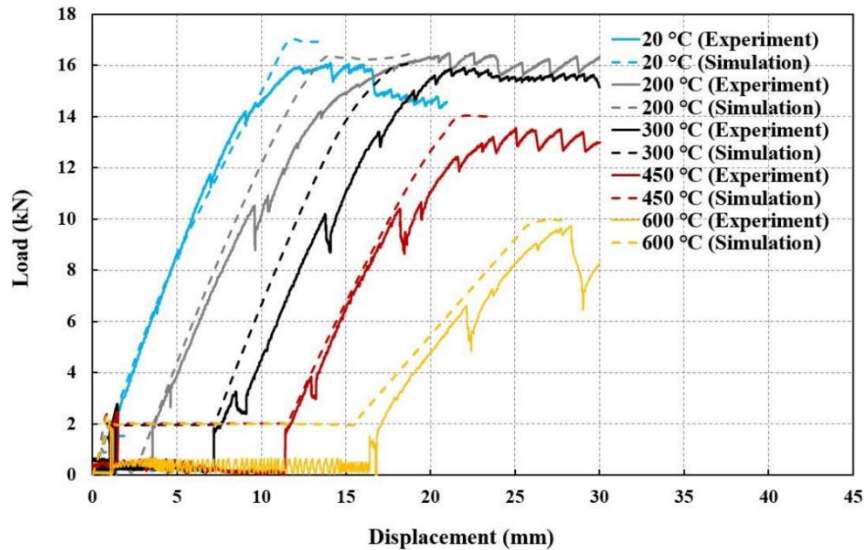


Fig. 11 - Comparison of load-displacement curves with MW panels 230 mm at different temperatures for experimental and numerical results

It is observed that the bending stiffness and bearing strengths predicted from FE models are in good agreement with the test results. During the tests, the loadings were stopped at some intervals to control the experimental conditions. These pauses caused some jumping (sharp movement) in the experimental curvatures. In Table 2, the maximum load and stiffness of sandwich panels at different temperatures are presented, where F_{max} and k_b are the maximum load and bending stiffness of sandwich panels for experimental and numerical results.

Table 2. The maximum load and stiffness of sandwich panels at different temperatures

Specimen	Temperature (°C)	Panel thickness (mm)	$F_{max,FEM}$ (kN)	$F_{max,EXP}$ (kN)	$k_{b,FEM}$ (kN/mm)	$k_{b,EXP}$ (kN/mm)
MW sandwich panel	20	100	8.60	9.28	0.82	0.84
	300	100	6.50	6.41	0.53	0.44
	450	100	4.95	4.53	0.37	0.32
	600	100	2.39	2.19	0.25	0.24
	20	230	16.91	16.51	1.49	1.55
	200	230	16.60	16.50	1.45	1.47
	300	230	16.05	15.90	1.44	1.46
	450	230	13.95	13.50	1.29	1.29
600	230	9.95	9.73	0.75	0.83	

2.4 Numerical and analytical parametric studies

2.4.1 General

After validating numerical simulations against the experimental results, an extensive number of finite element analyses are carried out to determine the bending stiffness of sandwich panels under bending loads at room and elevated temperatures. Simultaneously, an analytical study is conducted to compare the numerical and analytical results. The changes in dimensions of specimens are based on the commonly existing parts in the industry. For example, the facing thickness of sandwich panels usually ranges from 0.40 mm to 1.00 mm, or the core thickness changes between 50 mm and 300 mm. The material properties of the steel facings and the core in the parametric study are identical to those of tests.

In Table 3, the numerical and analytical results are presented and compared at different temperatures, where B , D and L are the width, thickness and span of panels, respectively, and F_b and F_t display the thickness of the lower and upper facings. The specimens are mainly categorized into four groups according to their temperatures. Each specimen is labelled by four segments in order to identify the core material, the parameter investigated, its size and the temperature of the exposed side. For instance, the label "MW-D-100-20" defines as follows. The first segment indicates the core material type, which is the MW core in this research. The second letter represents the parameter investigated; here,

"D" means the panel thickness. The third segment of the label shows the value of the panel thickness, and the fourth part of the label displays the temperature of the lower sheet. $k_{b,FEM}$ is the bending stiffness of panels obtained from the numerical results. According to 2.2, the bending stiffness of panels calculated by the analytical formulation is based on the two methods of the average shear modulus of the core and the shear modulus of the highest core temperature, which is a conservative approach for elevated temperatures. $k_{b,theory-avg}$ ("average solution") and $k_{b,theory-max}$ ("maximum solution"), respectively, indicate the bending stiffness calculated by the average shear modulus of the core and the shear modulus at the highest core temperature. It is evident that the "average" and "maximum" solutions give similar results at ambient temperature.

Table 3. Comparison of the bending stiffness of sandwich panels calculated by numerical and analytical methods

Specimens	B (mm)	D (mm)	F _b (mm)	F _t (mm)	L (mm)	$k_{b,theory-avg}$ (kN/mm)	$k_{b,FEM}$ (kN/mm)	$k_{b,theory-avg} / k_{b,FEM}$	$k_{b,theory-max}$ (kN/mm)	$k_{b,theory-max} / k_{b,FEM}$
MW-B-600-20	600	100	0.5	0.6	2500	0.36	0.41	0.88	0.36	0.88
MW-B-900-20	900	100	0.5	0.6	2500	0.54	0.62	0.87	0.54	0.87
MW-B-1200-20	1200	100	0.5	0.6	2500	0.72	0.83	0.87	0.72	0.87
MW-B-1500-20	1500	100	0.5	0.6	2500	0.90	1.04	0.87	0.90	0.87
MW-B-2500-20	2500	100	0.5	0.6	2500	1.5	1.50	1.00	1.50	1.00
MW-Fb-0.4-20	1200	100	0.4	0.6	2500	0.70	0.81	0.86	0.70	0.86
MW-Fb-0.5-20	1200	100	0.5	0.6	2500	0.72	0.83	0.87	0.72	0.87
MW-Fb-0.7-20	1200	100	0.7	0.6	2500	0.74	0.85	0.87	0.74	0.87
MW-Fb-1-20	1200	100	1	0.6	2500	0.76	0.87	0.87	0.76	0.87
MW-Ft-0.4-20	1200	100	0.5	0.4	2500	0.69	0.80	0.86	0.69	0.86
MW-Ft-0.7-20	1200	100	0.5	0.7	2500	0.73	0.84	0.87	0.73	0.87
MW-Ft-1-20	1200	100	0.5	1	2500	0.74	0.86	0.86	0.74	0.86
MW-L-1000-20	1200	100	0.5	0.6	1000	2.13	1.97	1.08	2.13	1.08
MW-L-1875-20	1200	100	0.5	0.6	1875	1.07	1.30	0.82	1.07	0.82
MW-L-2500-20	1200	100	0.5	0.6	2500	0.72	0.83	0.87	0.72	0.87
MW-L-3125-20	1200	100	0.5	0.6	3125	0.51	0.64	0.80	0.51	0.80
MW-L-4500-20	1200	100	0.5	0.6	4500	0.27	0.34	0.79	0.27	0.79
MW-L-6000-20	1200	100	0.5	0.6	6000	0.14	0.20	0.70	0.14	0.70
MW-D-50-20	1200	50	0.5	0.6	2500	0.30	0.38	0.79	0.30	0.79
MW-D-100-20	1200	100	0.5	0.6	2500	0.72	0.83	0.87	0.72	0.87
MW-D-160-20	1200	160	0.5	0.6	2500	1.24	1.31	0.95	1.24	0.95
MW-D-230-20	1200	230	0.5	0.6	2500	1.85	1.73	1.07	1.85	1.07
MW-D-300-20	1200	300	0.5	0.6	2500	2.47	2.06	1.20	2.47	1.20
MW-B-600-300	600	100	0.5	0.6	2500	0.25	0.27	0.93	0.19	0.70
MW-B-1200-300	1200	100	0.5	0.6	2500	0.50	0.53	0.94	0.38	0.72
MW-B-2500-300	2500	100	0.5	0.6	2500	1.04	1.11	0.94	0.80	0.72
MW-Fb-0.4-300	1200	100	0.4	0.6	2500	0.49	0.52	0.94	0.38	0.73
MW-Fb-0.7-300	1200	100	0.7	0.6	2500	0.52	0.55	0.95	0.39	0.71
MW-Fb-1-300	1200	100	1	0.6	2500	0.53	0.57	0.93	0.40	0.70
MW-Ft-0.4-300	1200	100	0.5	0.4	2500	0.48	0.52	0.92	0.37	0.71
MW-Ft-0.7-300	1200	100	0.5	0.7	2500	0.50	0.54	0.93	0.39	0.72
MW-Ft-1-300	1200	100	0.5	1	2500	0.51	0.55	0.93	0.39	0.71
MW-L-1000-300	1200	100	0.5	0.6	1000	1.44	1.33	1.08	1.08	0.81

MW-L-1875-300	1200	100	0.5	0.6	1875	0.73	0.83	0.88	0.56	0.67
MW-L-2500-300	1200	100	0.5	0.6	2500	0.50	0.53	0.94	0.38	0.72
MW-L-3125-300	1200	100	0.5	0.6	3125	0.36	0.42	0.86	0.28	0.67
MW-L-4500-300	1200	100	0.5	0.6	4500	0.19	0.24	0.79	0.16	0.67
MW-L-6000-300	1200	100	0.5	0.6	6000	0.11	0.15	0.73	0.09	0.60
MW-D-50-300	1200	50	0.5	0.6	2500	0.22	0.25	0.88	0.17	0.68
MW-D-100-300	1200	100	0.5	0.6	2500	0.50	0.53	0.94	0.38	0.72
MW-D-160-300	1200	160	0.5	0.6	2500	0.85	0.83	1.02	0.65	0.78
MW-D-230-300	1200	230	0.5	0.6	2500	1.26	1.16	1.09	0.95	0.82
MW-D-300-300	1200	300	0.5	0.6	2500	1.68	1.36	1.24	1.26	0.93
MW-B-600-450	600	100	0.5	0.6	2500	0.19	0.19	1.00	0.10	0.53
MW-B-1200-450	1200	100	0.5	0.6	2500	0.38	0.37	1.03	0.20	0.54
MW-B-2500-450	2500	100	0.5	0.6	2500	0.79	0.76	1.04	0.42	0.55
MW-Fb-0.4-450	1200	100	0.4	0.6	2500	0.37	0.36	1.03	0.19	0.53
MW-Fb-0.7-450	1200	100	0.7	0.6	2500	0.39	0.37	1.05	0.20	0.54
MW-Fb-1-450	1200	100	1	0.6	2500	0.40	0.40	1.00	0.20	0.50
MW-Ft-0.4-450	1200	100	0.5	0.4	2500	0.37	0.36	1.03	0.20	0.56
MW-Ft-0.7-450	1200	100	0.5	0.7	2500	0.38	0.37	1.03	0.20	0.54
MW-Ft-1-450	1200	100	0.5	1	2500	0.39	0.37	1.05	0.20	0.54
MW-L-1000-450	1200	100	0.5	0.6	1000	1.09	0.90	1.21	0.54	0.60
MW-L-1875-450	1200	100	0.5	0.6	1875	0.56	0.57	0.98	0.28	0.49
MW-L-2500-450	1200	100	0.5	0.6	2500	0.38	0.37	1.03	0.20	0.54
MW-L-3125-450	1200	100	0.5	0.6	3125	0.27	0.29	0.93	0.15	0.52
MW-L-4500-450	1200	100	0.5	0.6	4500	0.15	0.17	0.88	0.09	0.53
MW-L-6000-450	1200	100	0.5	0.6	6000	0.08	0.11	0.73	0.05	0.45
MW-D-50-450	1200	50	0.5	0.6	2500	0.16	0.17	0.94	0.09	0.53
MW-D-100-450	1200	100	0.5	0.6	2500	0.38	0.37	1.03	0.20	0.54
MW-D-160-450	1200	160	0.5	0.6	2500	0.65	0.55	1.18	0.33	0.60
MW-D-230-450	1200	230	0.5	0.6	2500	0.96	0.66	1.45	0.48	0.73
MW-D-300-450	1200	300	0.5	0.6	2500	1.28	0.86	1.49	0.64	0.74
MW-B-600-600	600	100	0.5	0.6	2500	0.13	0.14	0.93	0.09	0.64
MW-B-1200-600	1200	100	0.5	0.6	2500	0.27	0.27	1.00	0.19	0.70
MW-B-2500-600	2500	100	0.5	0.6	2500	0.58	0.56	1.04	0.40	0.71
MW-Fb-0.4-600	1200	100	0.4	0.6	2500	0.27	0.27	1.00	0.19	0.70
MW-Fb-0.7-600	1200	100	0.7	0.6	2500	0.29	0.28	1.04	0.20	0.71
MW-Fb-1-600	1200	100	1	0.6	2500	0.29	0.29	1.00	0.20	0.69

MW-Ft-0.4-600	1200	100	0.5	0.4	2500	0.27	0.27	1.00	0.19	0.70
MW-Ft-0.7-600	1200	100	0.5	0.7	2500	0.28	0.27	1.04	0.19	0.70
MW-Ft-1-600	1200	100	0.5	1	2500	0.28	0.28	1.00	0.19	0.68
MW-L-1000-600	1200	100	0.5	0.6	1000	0.80	0.63	1.27	0.53	0.84
MW-L-1875-600	1200	100	0.5	0.6	1875	0.41	0.42	0.98	0.28	0.67
MW-L-2500-600	1200	100	0.5	0.6	2500	0.27	0.27	1.00	0.19	0.70
MW-L-3125-600	1200	100	0.5	0.6	3125	0.20	0.22	0.91	0.14	0.64
MW-L-4500-600	1200	100	0.5	0.6	4500	0.10	0.13	0.77	0.08	0.62
MW-L-6000-600	1200	100	0.5	0.6	6000	0.06	0.08	0.75	0.05	0.63
MW-D-50-600	1200	50	0.5	0.6	2500	0.12	0.13	0.92	0.08	0.62
MW-D-100-600	1200	100	0.5	0.6	2500	0.27	0.27	1.00	0.19	0.70
MW-D-160-600	1200	160	0.5	0.6	2500	0.47	0.42	1.12	0.32	0.76
MW-D-230-600	1200	230	0.5	0.6	2500	0.70	0.47	1.49	0.47	1.00
MW-D-300-600	1200	300	0.5	0.6	2500	0.93	0.65	1.43	0.63	0.97

2.4.2 Effect of inner and outer sheet thickness

The sheet thickness of sandwich panels varies between 0.4 mm and 1.0 mm. According to Table 3, it can be concluded that the sheet thickness within the range above does not play a significant role in changing the bending stiffness of specimens. For example, at room temperature, when the inner sheet thickness changes from 0.4 mm to 1.0 mm, the stiffness of FE models increases only around 7.4%. This growth for analytical results is about 8.5%. Consequently, the sheet thickness of panels is not considered as a determining parameter to influence the bending stiffness. The comparison of the numerical and analytical results shows that stiffness calculated by the analytical solution is favourably less than numerical ones (Fig. 12). In fact, the analytical results lead to a safe prediction for bending stiffness. Furthermore, the growth rate of both methods (analytical and FE approaches) is similar.

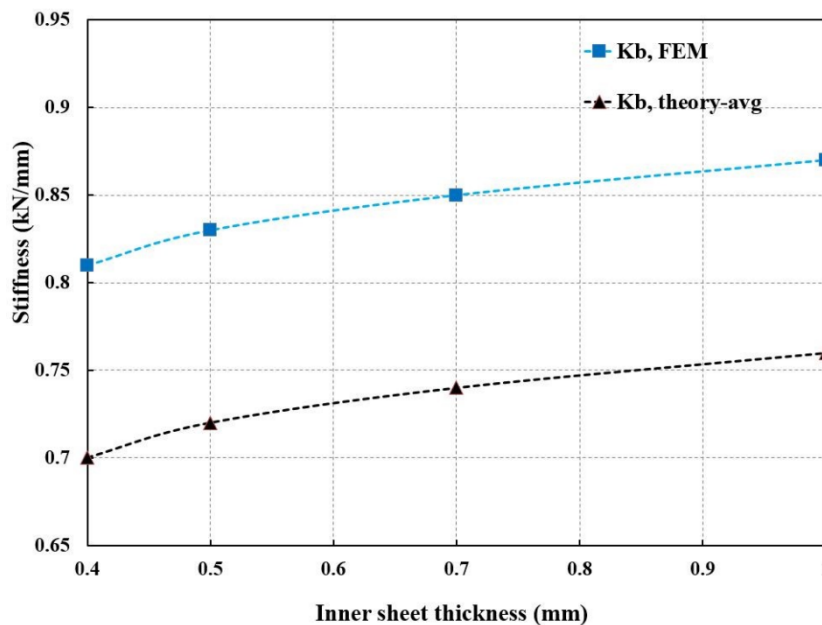


Fig. 12 - Bending stiffness of numerical and analytical results with different inner sheet thicknesses at ambient temperature

2.4.3 Effect of panel thickness

One of the significant parameters to determine the bending stiffness is the sandwich panel thickness. Fig. 13 indicates the load-displacement curves of MW-L-2500-20 specimens taken from simulations with different thicknesses at ambient temperature. As expected, with the increase of the thickness, the stiffness increases. For instance, the stiffness of a panel with 300 mm thickness is around 5.4 times greater than the same panel with 50 mm thickness. The bending stiffness values calculated by the analytical and numerical methods are very similar for the panels with a thickness of less than 160 mm (Fig. 14). However, for the panels thicker than 160 mm, the values of numerical results are less than analytical results.

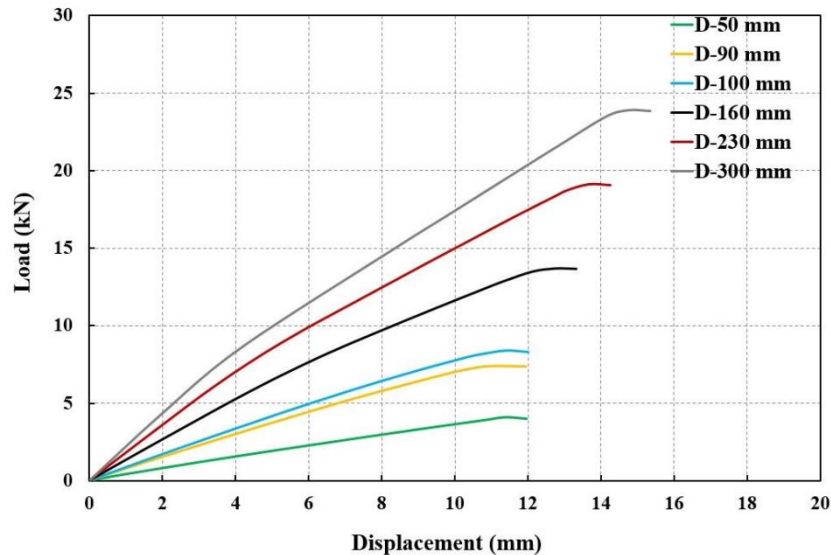


Fig. 13 - Load-displacement curves for MW-L-2500-20 specimen different panel thicknesses at ambient temperature

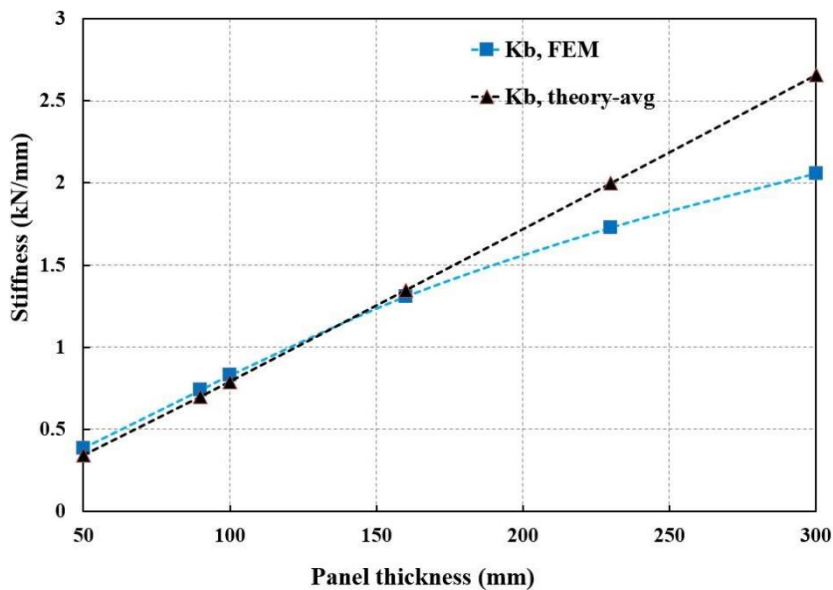


Fig. 14 - Bending stiffness of numerical and analytical results with different panel thicknesses at ambient temperature

2.4.4 Effect of panel width

In this study, the panel width varies from 600 mm to 2500 mm. Fig. 15 demonstrates that the panel width directly affects the bending stiffness. When the panel width increases around 67%, the stiffness grows about 68%. Fig. 16 better illustrates the fact that there is almost a linear relationship between the panel width and bending stiffness for both analytical and numerical results. Furthermore, it can be concluded that up to 1800 mm width, the analytical results are on the safe side, while for higher values, the analytical results are non-conservative compared to the simulations.

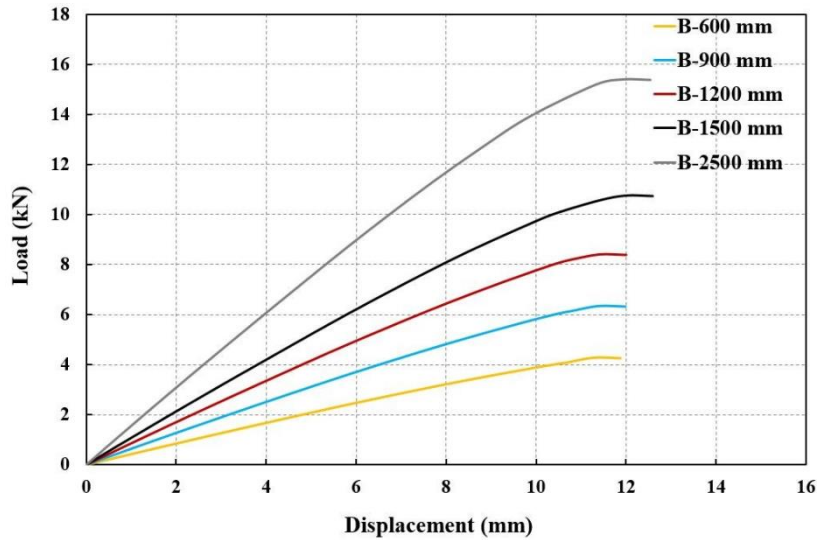


Fig. 15 - Load-displacement curves for MW-L-2500-20 specimen different panel widths at ambient temperature

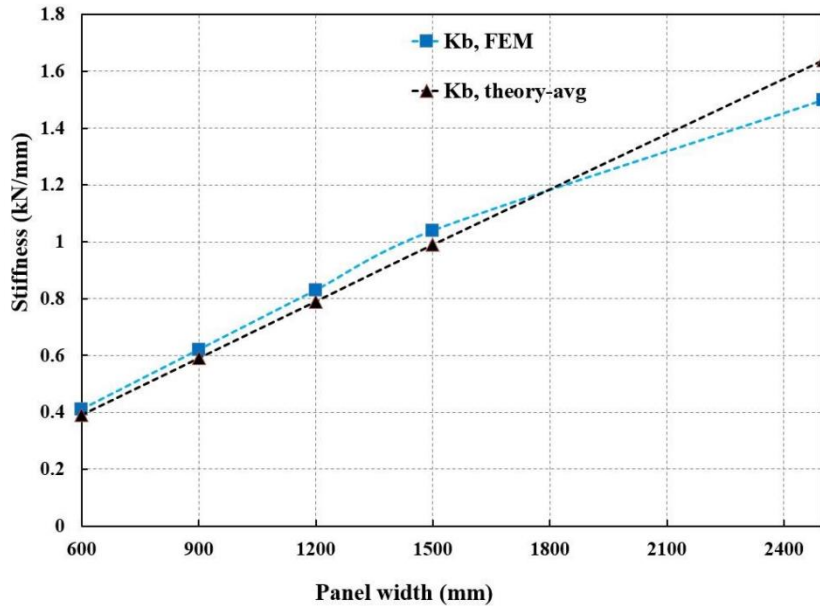


Fig. 16 - Bending stiffness of numerical and analytical results with different panel widths at ambient temperature

2.4.5 Effect of panel spans

According to the results obtained from the finite element models, it is found that changing the panel span has a substantial influence on the bending stiffness of panels. In fact, it can be said that with the enlargement of the span, the stiffness decreases. The shortest panel in this research has a 1000 mm length with 1.97 kN/mm stiffness, which with increasing its length to 2500 mm and 6000 mm, the bending stiffness of panels reduces to 0.83 kN/mm and 0.20 kN/mm, respectively. As can be seen in Fig. 17, the process of changing stiffness is similar for both analytical and numerical results, and the analytical results for all amounts are slightly less than simulations. Therefore, it can be concluded that for all spans length, the analytical solution is safe.

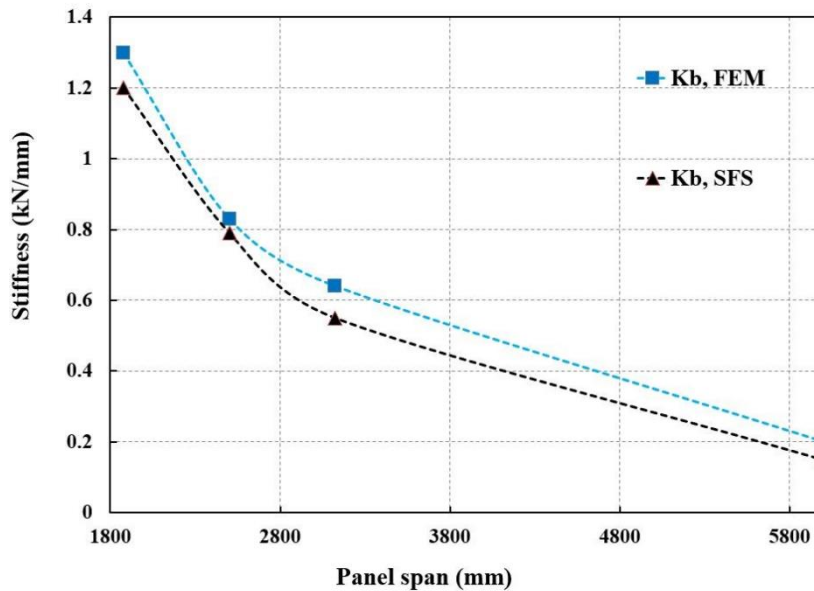


Fig. 17 - Bending stiffness of numerical and analytical results with different panel spans at ambient temperature

2.4.6 Effect of temperature

As shown in Table 3, different temperatures are assigned to the lower sheet of panels to evaluate the fire's effect on the bending stiffness. As expected, at elevated temperatures, the stiffness and the load-bearing capacity are reduced for numerical and analytical results. This decrease is due to the degradation in the lower sheet and the core mechanical properties. Fig. 18, as an example, illustrates the numerical results for MW-B-1200-20 specimens at different temperatures.

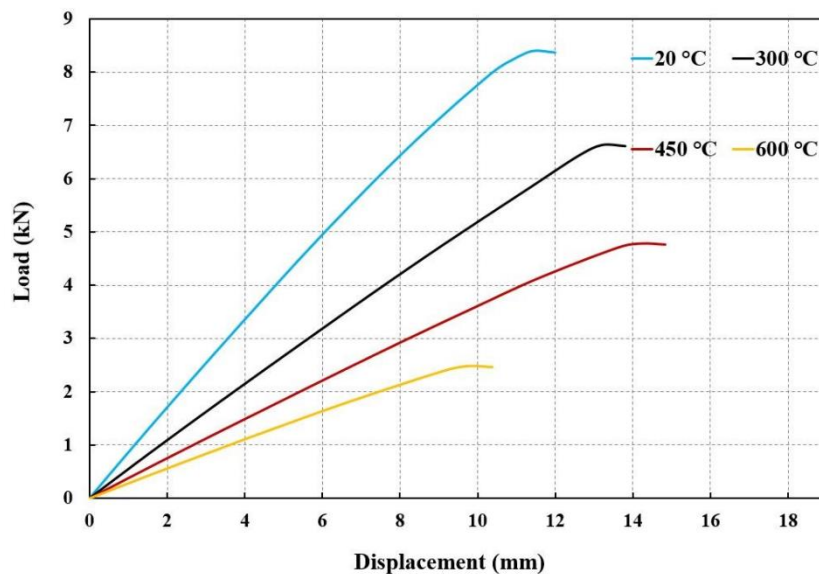


Fig. 18 - Load-displacement curves for MW-B-1200-20 specimen at different temperatures

Fig. 19 indicates the bending stiffness of numerical and analytical results for MW-B-1200-20 specimens at different temperatures. The stiffness calculated by all methods decreases with increasing the temperature. Nevertheless, the rate of reduction varies for them. In the case of the "average solution", the numerical and analytical results become closer as the temperature elevates. However, up to 450 °C, the stiffness drop of the analytical results calculated by the "maximum solution" is approximately parallel to the numerical results.

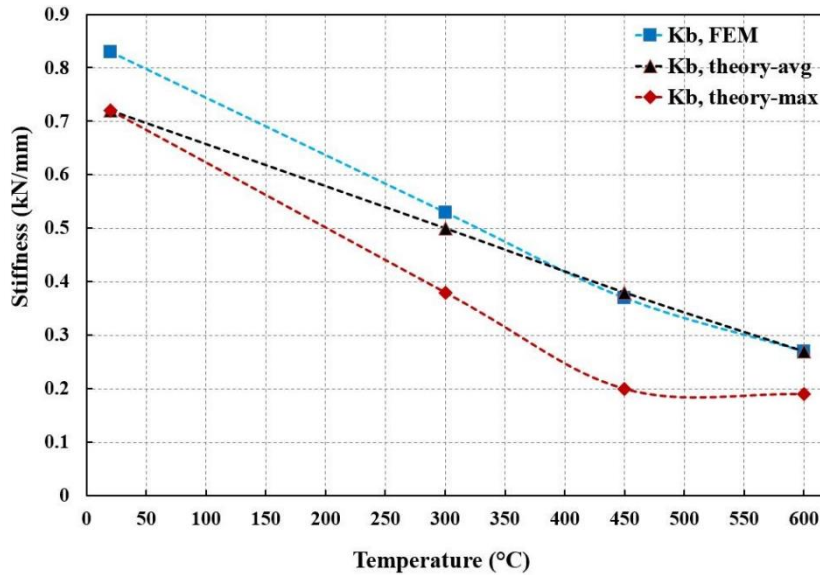


Fig. 19 - Bending stiffness of numerical and analytical results for MW-B-1200-20 specimen at different temperatures

3 Results and Discussion

In the previous sections, the effect of each parameter at ambient temperature was investigated. In this part, the influence of parameter changes on the bending stiffness at different temperatures for simulations as well as analytical solutions is studied and compared. In Fig. 20, the bending stiffness of panels with various panel thicknesses at different temperatures is shown by numerical and analytical approaches. In this section, when the analytical solution is mentioned, it refers to the "average solution". With increasing the temperature, as shown in Fig. 20, the difference between bending stiffness values of the panels with various thicknesses decreases. In other words, at higher temperatures, the stiffness values tend to converge. The same phenomenon happens for panels with different spans and widths. Indeed, as the temperature elevates, the bending stiffness values approach (Fig. 21).

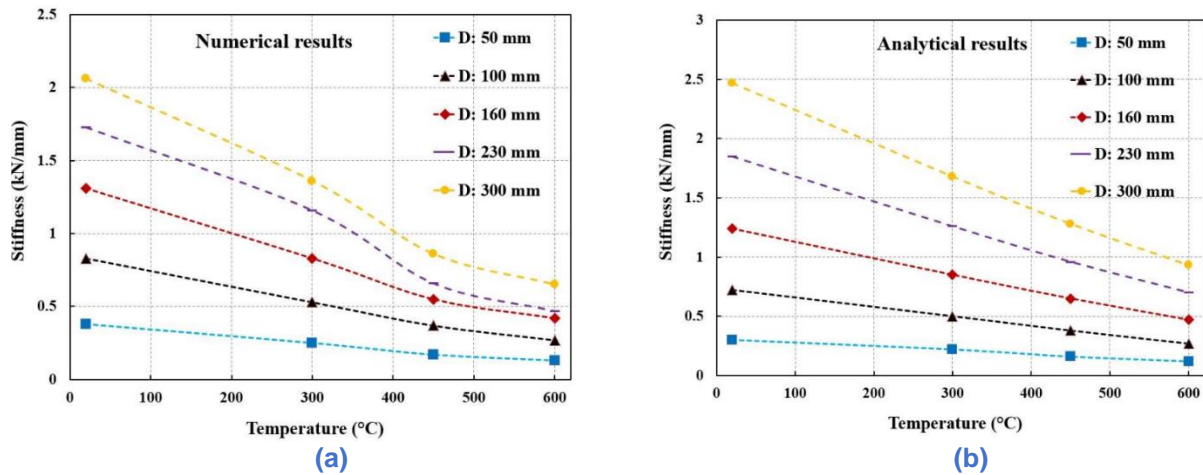


Fig. 20 - Bending stiffness of sandwich panels with various thicknesses at different temperatures, a) numerical results, and b) analytical results

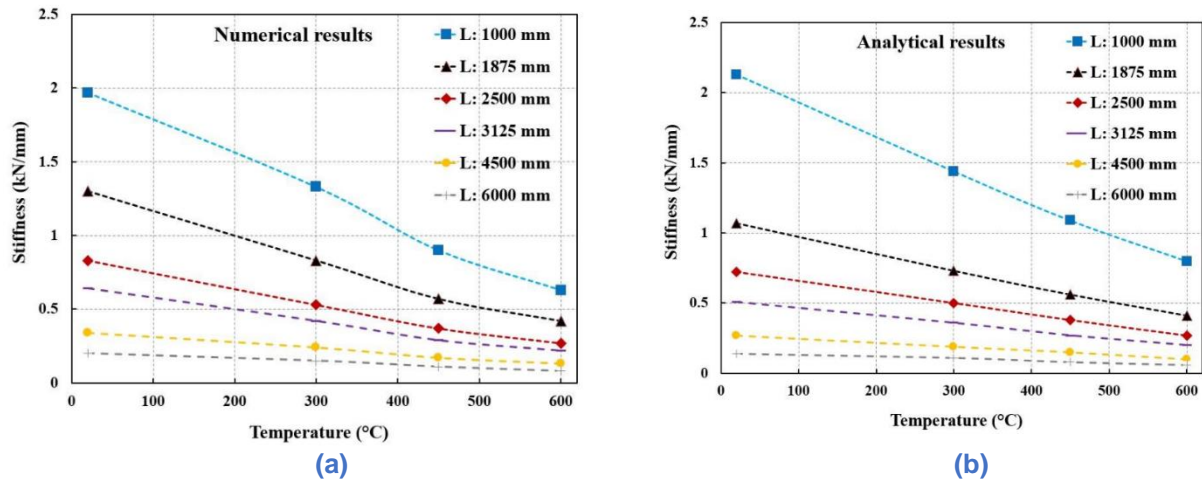


Fig. 21 - Bending stiffness of sandwich panels with various spans at different temperatures, a) numerical results, and b) analytical results

To evaluate the proposed solutions at elevated temperatures, Fig. 22 compares the stiffness calculated by the simulation, the "average solution", and the "maximum solution" for the panels with different widths of 600 mm, 1200 mm and 2500 mm. It is observed that the results calculated by the "average solution" for different widths are very close to the stiffness values achieved from simulations. However, at higher temperatures (450 °C and 600 °C) for the wider panels, the "average solution" values are slightly greater than numerical values. Nevertheless, the "maximum solution" can be considered as an utterly conservative method.

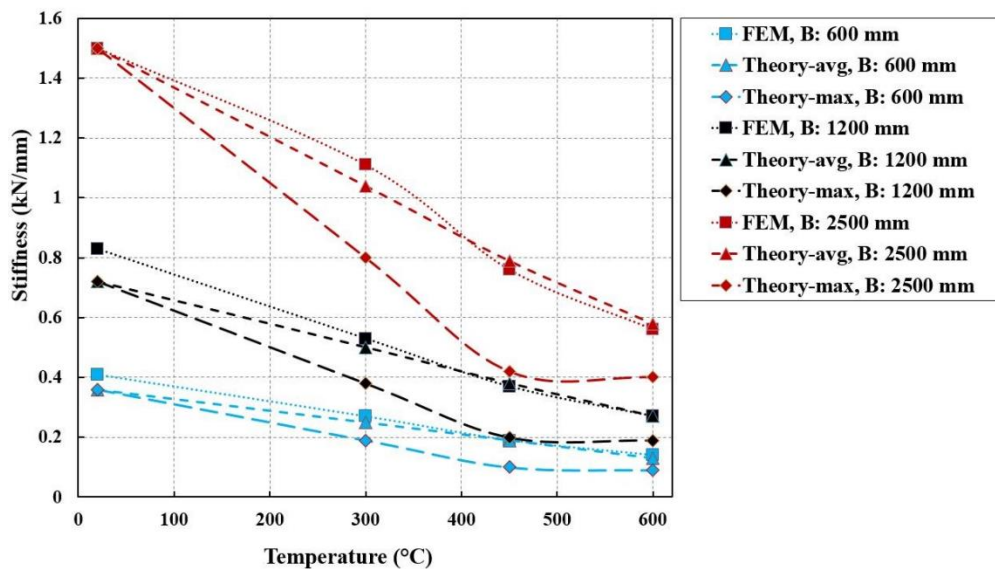


Fig. 22 - Bending stiffness of sandwich panels with various widths at different temperatures calculated by three methods

4 Conclusion

In the present study, the bending stiffness of sandwich panels under bending loadings at normal and elevated temperatures has been investigated. A FE model was developed to verify simulations with experimental results. After verifying simulations, a comprehensive parametric study at different temperatures was performed to investigate the effect of various parameters, such as panel span, width and thickness, on the bending stiffness of specimens. The geometrical and material nonlinearity for models was considered. The numerical results were compared with the analytical formulations provided by Eurocodes (EN 14509, 2013) at ambient temperature.

Moreover, the analytical formulations were developed to apply at elevated temperatures. For that reason, two methods called "average solution" and "maximum solution" were proposed. Based on the paper, the following conclusions can be drawn;

1. Although the panels become stiffer as the thickness of the inner and outer sheets increases, such a change is not noticeable. That could be because a change in sheet thickness does not lead to a significant difference in the moment of inertia for the panel cross-section. Since the panels' stiffness depends strongly on the moment of inertia of the panel cross-section, no significant change is observed in this case. The stiffness growth is similar for numerical and analytical results within the range of 0.40 mm to 1.00 mm thickness (around 8% only).
2. The thickness of the panels is one of the most effective parameters to determine panel stiffness. At room temperature, when the thickness of the panel increases from 50 mm to 100 mm, the bending stiffness calculated by simulation increases 2.18 times. Up to 160 mm panel thickness, the stiffness values calculated by numerical and analytical methods give approximately the same results at normal conditions; however, for thicker panels, the analytical results are slightly higher than numerical ones. Therefore, it can be concluded that for the panels with a thickness of less than 160 mm, the analytical solutions have better accuracy.
3. Increasing the width of panels leads to the higher bending stiffness values of sandwich panels. For analytical and numerical results, there is an almost linear relationship between bending stiffness and panel width. However, the growth rate of analytical results is slightly higher than the numerical results. According to the obtained results, at ambient temperature, it seems that up to 1800 mm panel width, the analytical results are slightly less than numerical results.
4. There is an inverse relationship between the panel span and the bending stiffness of panels. Indeed, the increase of panel span causes a reduction in the stiffness of panels. Nevertheless, this decrease is not linear. It is observed that for different span lengths, the analytical results are less than numerical ones.
5. In general, at higher temperatures, the stiffness of panels reduces. On the other hand, at elevated temperatures, the differences between stiffness values of various parameters decrease. For instance, the difference in bending stiffness values between the panels with different thicknesses at room temperature is higher than the difference between those stiffness values at 600 °C. This fact also applies to the panel span and width values.
6. In this study, two analytical solutions are proposed for elevated temperatures. The "average solution" offers a good approximation of numerical results. At temperatures higher than 450 °C, the "average solution" shows greater values than numerical results; nonetheless, this difference is not significant. The "maximum solution" presents very conservative results compared to the simulations, especially at temperatures higher than 450 °C. Consequently, applying the "average solution" seems a reasonable method to estimate the bending stiffness of sandwich panels.

5 Acknowledgement

The research is a part of the corresponding author's doctoral dissertation supported by the German Academic Exchange Service (DAAD). The tests have received funding from the Research Fund for Coal and Steel under grant agreement No 751583.

The authors would like to express great thanks to Prof. F. Wald and his colleagues from the Department of Steel and Timber Structures, CVUT Prague, who carried out the bending tests in the laboratory of the Faculty of Civil Engineering. We would like to thank the other partners from the STABFI project (BME Budapest, CITY London, RUUKKI, HAMK and SFS, Finland, and Kingspan, Czech Republic) for their helpful discussions.

References

1. Steel cladding systems for stabilization of steel buildings in fire 2020.
2. Rahimijonoush, A., Bayat, M. Experimental and numerical studies on the ballistic impact response of titanium sandwich panels with different facesheets thickness ratios. *Thin-Walled Structures*. 2020. 157. Pp. 107079. DOI:10.1016/j.tws.2020.107079.
3. The Behavior of Sandwich Structures of Isotropic and Composite Material. .
4. Farrokhabadi, A., Ahmad Taghizadeh, S., Madadi, H., Norouzi, H., Ataei, A. Experimental and numerical analysis of novel multi-layer sandwich panels under three point bending load. *Composite Structures*. 2020. 250. Pp. 112631. DOI:10.1016/j.compstruct.2020.112631.
5. Noor, A.K., Burton, W.S., Bert, C.W. Computational models for sandwich panels and shells. *Applied Mechanics Reviews*. 1996. 49(3). Pp. 155–199. DOI:10.1115/1.3101923.
6. Colombo, I.G., Colombo, M., di Prisco, M., Pouyaei, F. Analytical and numerical prediction of the bending behaviour of textile reinforced concrete sandwich beams. *Journal of Building Engineering*. 2018. 17. Pp. 183–195. DOI:10.1016/j.jobe.2018.02.012.
7. Juntikka, R., Hallstrom, S. Shear Characterization of Sandwich Core Materials Using Four-point Bending. *Journal of Sandwich Structures & Materials*. 2007. 9(1). Pp. 67–94. DOI:10.1177/1099636207070574.
8. Huang, S., Samali, B., Li, J. Numerical and experimental investigations of a thermal break composite façade mullion under four-point bending. *Journal of Building Engineering*. 2021. 34. Pp. 101590. DOI:10.1016/j.jobe.2020.101590.
9. Elmushyakh, A. Collapse mechanisms of out-of-plane preload composite sandwich beams under in-plane loading. *Journal of Building Engineering*. 2019. 26. Pp. 100875. DOI:10.1016/j.jobe.2019.100875.
10. Taghipoor, H., Eyvazian, A., Musharavati, F., Sebaey, T.A., Ghiaskar, A. Experimental investigation of the three-point bending properties of sandwich beams with polyurethane foam-filled lattice cores. *Structures*. 2020. 28. Pp. 424–432. DOI:10.1016/j.istruc.2020.08.082.
11. Kazemi, M. Experimental analysis of sandwich composite beams under three-point bending with an emphasis on the layering effects of foam core. *Structures*. 2021. 29. Pp. 383–391. DOI:10.1016/j.istruc.2020.11.048.
12. Mofrad, A.S., Shlychkova, D., Ciupack, Y., Pasternak, H. Evaluating bending stiffness and resistance of sandwich panels at elevated temperatures. DOI:10.3846/mbmst.2019.032.
13. Shoushtarian Mofrad, A., Pasternak, H. BEHAVIOUR OF MINERAL WOOL SANDWICH PANELS UNDER BENDING LOAD AT ROOM AND ELEVATED TEMPERATURES. *Engineering Structures and Technologies*. 2020. 12(1). Pp. 25–31. DOI:10.3846/est.2020.14046.
14. Srivaro, S., Matan, N., Lam, F. Stiffness and strength of oil palm wood core sandwich panel under center point bending. *Materials and Design*. 2015. 84. Pp. 154–162. DOI:10.1016/j.matdes.2015.06.097.
15. Daniel Ronald Joseph, J., Prabakar, J., Alagusundaramoorthy, P. Flexural behavior of precast concrete sandwich panels under different loading conditions such as punching and bending. *Alexandria Engineering Journal*. 2018. 57(1). Pp. 309–320. DOI:10.1016/j.aej.2016.11.016.
16. Michel Murillo, A., Tutikian, B.F., Christ, R., Silva, L.F.O., Maschen, M., Leandro Gómez, P., Oliveira, M.L.S. Analysis of the influence of thickness on fire reaction performance in polyisocyanurate core sandwich panels. *Journal of Materials Research and Technology*. 2020. 9(5). Pp. 9487–9497. DOI:10.1016/j.jmrt.2020.06.088.
17. Iyer, S.V., Chatterjee, R., Ramya, M., Suresh, E., Padmanabhan, K. A Comparative Study of the Three Point and Four Point Bending Behaviour of Rigid Foam Core Glass/Epoxy Face Sheet Sandwich Composites. *Materials Today: Proceedings*. 2018. 5(5). Pp. 12083–12090. DOI:10.1016/j.matpr.2018.02.184.
18. BS EN 14509:2013 - Self-supporting double skin metal faced insulating panels. Factory made products. Specifications. .
19. Cábová K., Arha T., Lišková N., W.F. Experimental investigation of stiffness in bending of sandwich panels at elevated temperatures. 2019. Pp. 1–6.
20. Dassault Systemes. ABAQUS2017.
21. Yan, J.B., Guan, H.N., Wang, T. Finite element analysis for flexural behaviours of SCS sandwich beams with novel enhanced C-channel connectors. *Journal of Building Engineering*. 2020. 31. Pp. 101439. DOI:10.1016/j.jobe.2020.101439.

Shoushtarian Mofrad A., Hartmut P.

Numerical and analytical study on bending stiffness of sandwich panels at ambient and elevated temperatures; 2021; *Construction of Unique Buildings and Structures*; 94 Article No 9405. doi: 10.4123/CUBS.94.5

22. Craveiro, H.D., Rodrigues, J.P.C., Santiago, A., Laím, L. Review of the high temperature mechanical and thermal properties of the steels used in cold formed steel structures - The case of the S280 Gd+Z steel. *Thin-Walled Structures*. 2016. 98. Pp. 154–168. DOI:10.1016/j.tws.2015.06.002.
23. EN 1993-1-2: Eurocode 3: Design of steel structures - Part 1-2: General rules - Structural fire design 1993.
24. Gnip, I., Vėjelis, S., Keršulis, V., Vaitkus, S. Strength and deformability of mineral wool slabs under short-term compressive, tensile and shear loads. *Construction and Building Materials*. 2010. 24(11). Pp. 2124–2134. DOI:10.1016/j.conbuildmat.2010.04.047. URL: <https://linkinghub.elsevier.com/retrieve/pii/S0950061810001686> (date of application: 5.03.2021).
25. Mihlayanlar, E., Dilmaç, Ş., Güner, A. Analysis of the effect of production process parameters and density of expanded polystyrene insulation boards on mechanical properties and thermal conductivity. *Materials and Design*. 2008. 29(2). Pp. 344–352. DOI:10.1016/j.matdes.2007.01.032.
26. Liu, F., Fu, F., Wang, Y., Liu, Q. Fire performance of non-load-bearing light-gauge slotted steel stud walls. *Journal of Constructional Steel Research*. 2017. 137. Pp. 228–241. DOI:10.1016/j.jcsr.2017.06.034.
27. Mao, W.J., Wang, W. Da, Xian, W. Numerical analysis on fire performance of steel-reinforced concrete-filled steel tubular columns with square cross-section. *Structures*. 2020. 28. Pp. 1–16. DOI:10.1016/j.istruc.2020.08.043.
28. Li, Z., Chen, W., Hao, H. Numerical study of sandwich panel with a new bi-directional Load-Self-Cancelling (LSC) core under blast loading. *Thin-Walled Structures*. 2018. 127. Pp. 90–101. DOI:10.1016/j.tws.2018.02.003.
29. Wang, Y. jing, Zhang, Z. jia, Xue, X. min, Zhang, L. Free vibration analysis of composite sandwich panels with hierarchical honeycomb sandwich core. *Thin-Walled Structures*. 2019. 145. Pp. 106425. DOI:10.1016/j.tws.2019.106425.
30. Seo, J., Won, D., Kim, S., Kang, Y.J. Inelastic compressive buckling behavior of a cylindrical shell at elevated temperature: Case study. *Journal of Building Engineering*. 2019. 24. Pp. 100766. DOI:10.1016/j.jobbe.2019.100766.
31. Pournaghshband, A., Afshan, S., Theofanous, M. Elevated temperature performance of restrained stainless steel beams. *Structures*. 2019. 22. Pp. 278–290. DOI:10.1016/j.istruc.2019.08.015.
32. Ding, R., Fan, S., Chen, G., Li, C., Du, E., Liu, C. Fire resistance design method for restrained stainless steel H-section columns under axial compression. *Fire Safety Journal*. 2019. 108. Pp. 102837. DOI:10.1016/j.firesaf.2019.102837.
33. Olteanu, I., Ciongradi, I.-P., Anechitei, M., Budescu, M. The ductile design concept for seismic actions in miscellaneous design codes. *Buletinul Institutului Politehnic din Iași, Tomul LV (LIX), Fasc. 4. Secția Construcții. Arhitectură*. 2009. Pp. 55–62.